ECS Transactions, 50 (2) 1807-1814 (2012)
10.1149/05002.1807ecst ©The Electrochemical Society

Electrospun Iron/Polyacrylonitrile Derived Nanofibrous Catalysts for Oxygen Reduction Reaction

J. Wu[a], D. Higgins[a], and Z. Chen[a*]

[a] Department of Chemical Engineering, Waterloo Institute of Nanotechnology, University of Waterloo, Waterloo, Ontario N2L3G1, Canada

In the current work, non-precious nanofibrous catalysts were prepared by electrospinning a solution of iron acetate and polyacrylonitrile and subjecting the electrospun fibers to high temperature pyrolysis. The resulting nanofibrous catalysts were evaluated for their ORR activity and characterized via SEM, BET surface area analysis, and XPS. The nanofibrous catalysts were also acid leached and exposed to a second high temperature pyrolysis. The acid leached and re-pyrolyzed catalyst showed improved ORR activity. Physical characterization of the re-pyrolyzed catalyst suggests that the catalyst exhibits higher ORR activity that may be due to increased surface area and micropore volume.

Introduction

Proton Exchange Membrane Fuel Cells (PEMFCs) are a promising technology in delivering sustainable energy due to their high efficiency, high power density, and low operating temperature (1). PEMFCs are applicable in a wide variety of energy applications including portable electronic devices, localized power generators, and electric vehicles. The oxygen reduction reaction (ORR) occurs at the cathode of the PEMFC and is significantly slower than the corresponding anodic reaction (2-5). As a result, greater amount of catalyst is needed at the cathode. Platinum catalysts are employed to catalyze the slow ORR occurring at the cathode. Although platinum catalysts are highly effective and stable in the harsh acidic environments of PEMFCs, the high cost introduced by the use of the precious metal greatly inhibits widespread adoption of the technology. The development of inexpensive non-precious ORR catalysts is a necessity in reducing the material cost of the PEMFC and ensuring the PEMFC as an attractive option.

Transmission metal macrocyclic complexes (6-8), such as iron phthalocyanine, have been found to naturally exhibit catalytic activity towards ORR. High temperature pyrolysis of these compounds has also been shown to improve the activity and stability of these catalysts in acidic conditions (9-14). Following this work, it was shown that pyrolysis of separate cheaper pre-cursors containing carbon, nitrogen, and iron produces a catalyst active towards ORR (15,16). These non-precious catalysts are highly promising and are capable of exhibiting performances close to that of commercially available platinum catalysts (5,17).

In the current work, nanofibrous pyrolyzed catalyst using iron and polyacrylonitrile as both a carbon and nitrogen source are synthesized and evaluated for their catalytic

activity. A solution containing polyacrylonitrile and iron acetate was electrospun to form the nanofiber morphology. After stabilizing the fibers in air, the fibers undergo high temperature pyrolysis, producing highly conductive carbon nanofibers that are also active towards ORR. These nanofibrous catalysts (FePAN4-900) can also be arranged into a porous electrode structure, allowing for excellent mass transport properties for the reactants of a PEMFC. To improve the activity of the catalyst, the catalyst undergoes a second high temperature pyrolysis treatment after acid leaching (FePAN4-900-AH), resulting in porous nanofibers. The acid treatment involves immersing the nanofibrous catalysts in 0.5 M H_2SO_4 with constant stirring for a total of 24 hours. Although this treatment followed by a second high temperature prolysis results in catalysts with higher activity, it is difficult to predict the outcome the treatment will have on the durability of the catalysts. For the present work, both catalysts were evaluated for their electrochemical activity towards ORR and physically characterized via SEM imaging and BET analysis. The durability of the catalysts is to be investigated in future work.

Experimental details

Synthesis of FePAN4-900 non-precious catalyst

FePAN4-900 catalysts were synthesized by electrospinning a solution containing 5 wt% polyacrylonitrile and 0.2 wt% iron(II) acetate in DMF. The solution was electrospun at a distance of 13 cm from the collector electrode to the tip of the spinneret at an injection rate of 0.008 mL/min with applied potential of 13 kV. After spinning, the electrospun fibers are allowed to dry and are collected. The fibers undergo stabilization in air at 250 °C for 3 hours at a heating rate of 5 °C/min. Once stabilized, the fibers are heated to 900 °C at a rate of 5 °C/min, undergoing high temperature pyrolysis.

Synthesis of FePAN4-900-AH non-precious catalyst (acid treatment of FePAN4-900)

FePAN4-900 catalysts are taken and acid leached in 0.5 M H_2SO_4 for 24 hours at 80 °C with constant stirring. The catalysts are then filtrated, washed, and allowed to dry before undergoing a second high temperature pyrolysis at 900 °C with a heating rate of 5 °C/min, resulting in porous FePAN4-900-AH catalysts.

Catalyst characterization

Electrochemical characterization. Both FePAN4-900 and FePAN4-900-AH catalysts were electrochemically characterized by employing a rotating disk electrode system and a potentiostat. Catalyst inks were prepared by dispersing 2 mg of catalyst in 1 mL of ethanol. An 8 µL aliquot of ink was deposited onto the surface of a glassy carbon electrode five times before adding 8 µL of 0.5 wt% Nafion solution. The electrode was submerged in a electrochemical cell containing 0.1 M $HClO_4$ and half-cell measurements were taken using a Ag/AgCl reference electrode and a platinum wire counter electrode. Polarization curves were taken for each catalyst after saturating the cell with O_2 gas to evaluate the catalyst's ORR performance. The background current was taken after saturating the cell with N_2 gas.

Physical characterization. The overall fibrous morphology of both catalysts was examined via SEM imaging. The BET surface areas, BJH desorption average pore size, and micropore volume (using H-K method) of both catalysts were obtained via analysis of the BET nitrogen adsorption/desorption isotherms of the catalysts. Both catalysts were degassed at 250 °C for 12 hours before obtaining the nitrogen adsorption/desorption isotherms. The surface composition of both catalysts were examined via XPS analysis conducted on the N 1s, and Fe $2p_{2/3}$ lines at a take-off angle of 90° using an Al Kα X-ray source with a spot size of 400 μm.

Results and discussion

SEM analysis of nanofibrous catalysts

SEM imaging of both FePAN4-900 and FePAN4-900-AH catalysts was conducted to confirm the structural morphology of the catalysts. Figure 1 shows SEM images of the electrospun fibers prior to high temperature pyrolysis, and the ORR active carbon nanofibers prior and post acid leaching. Due to the electrospinning technique, the catalysts consist of a mesh of anisotropic catalytically active carbon nanofibers with diameters ranging from 100-200 nm. This mesh arrangement can potentially allow for excellent mass transport of reactants to the active sites of the catalyst. The SEM images of the pyrolyzed catalysts also show agglomeration of iron into small particles due to inevitable sintering as a result of the high temperature treatment. These small agglomerated iron particles could diminish the ORR activity of the catalyst by blocking ORR active sites. Lastly, the SEM images show that the catalyst maintains its nanofibrous morphology after pyrolysis of the electrospun fibers. Additionally, this nanofibrous morphology is retained after acid leaching and re-pyrolysis of the catalysts.

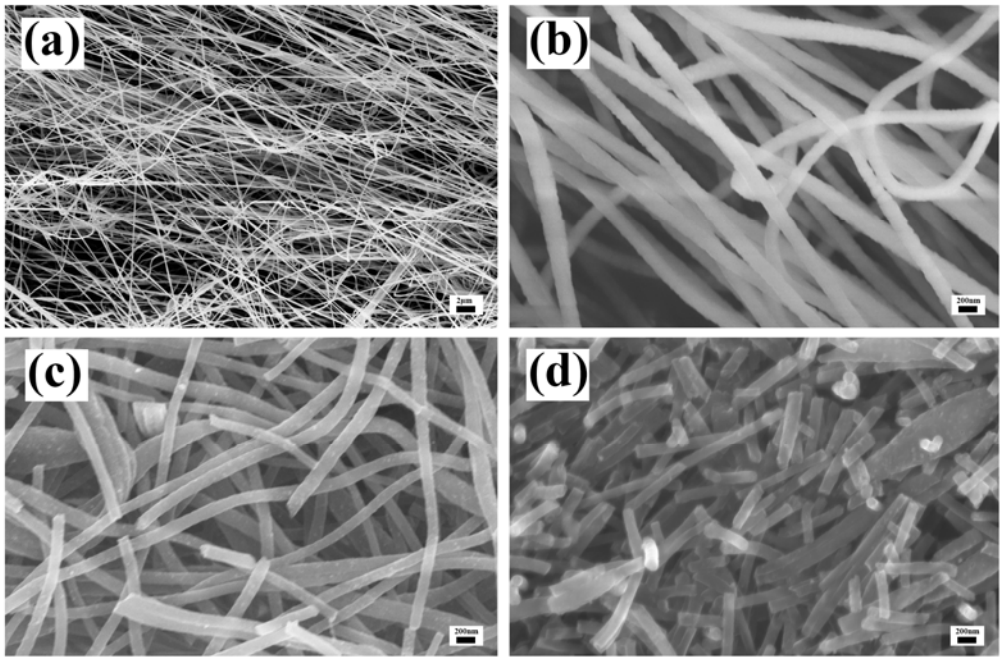

Figure 1. SEM images of (a, b) electrospun iron/polyacrylonitrile fibers, (c) FePAN4-900 nanofibrous catalyst, and (d) FePAN4-900-AH nanofibrous catalyst.

Electrochemical half-cell performance

The electrochemical half-cell polarization curves of both FePAN4-900 and FePAN4-900-AH are shown in figure 2 obtained at 100 RPM, 400 RPM, 900 RPM and 1600 RPM. Both catalysts exhibit well defined limiting currents at all rotation speeds.

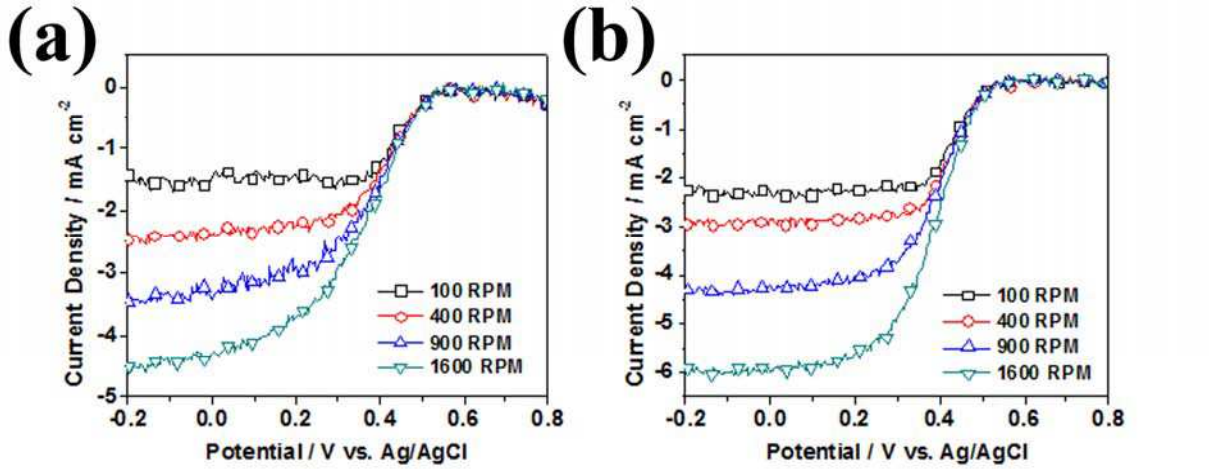

Figure 2. Polarization curves of (a) FePAN4-900 and (b) FePAN4-900-AH obtained in O_2 saturated 0.1 M $HClO_4$.

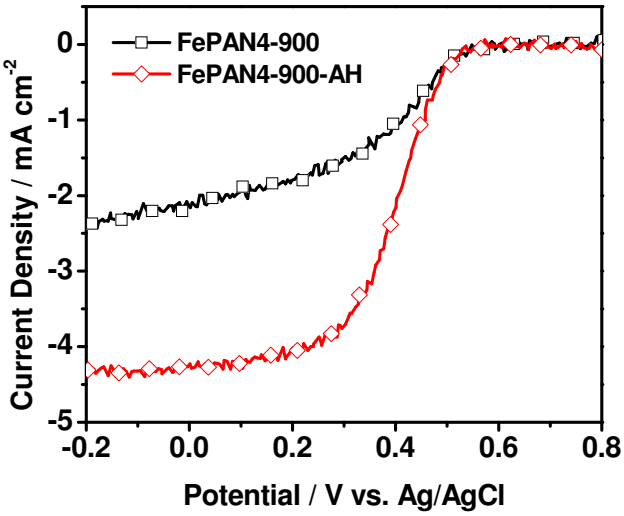

Figure 3. Comparison of ORR activity of (a) FePAN4-900 and (b) FePAN4-900-AH in O_2 saturated 0.1 M $HClO_4$ at 900 RPM.

A direct comparison of the two catalysts at 900 RPM can be seen in figure 3. From figure 3, it can be seen that the acid leaching and re-pyrolysis of the FePAN4-900 catalyst resulted in significant improvements in both the limiting current and half-wave potential. The on-set potential of both catalysts remain identical at approximately 0.57 V vs. Ag/AgCl. The limiting current exhibits the most profound improvement with the FePAN4-900-AH catalyst showing 1.8x higher limiting currents over the FePAN4-900 catalyst. The improvements in catalytic activity occur in the mass transport limited regions of the polarization curve, while the purely kinetic region of the catalyst (the on-set potential) is indistinguishable between the two catalysts. This observation suggests that the acid leaching and re-pyrolysis of the FePAN4-900 catalyst, producing the FePAN4-900-AH catalyst, largely results in a physical change in the microstructure of the catalyst with far less influence on the structure of the ORR active site. Both XPS and BET analyses of the two catalysts strongly support this hypothesis.

N 1s and Fe $2p_{2/3}$ XPS analysis

The N 1s and Fe $2p_{2/3}$ spectra were taken to examine the surface active site composition of both the FePAN4-900 and FePAN4-900-AH catalysts. Both nitrogen and iron are thought to be essential in the formation of ORR active sites after pyrolysis (18-20). Research into a type of pyrolyzed non-precious catalysts suggests that nitrogen and iron may be part of the active site composition (18,19). The ORR active site of these catalysts has been previously proposed to be located within the micropores (19) of the catalyst comprising of FeN_4/C moieties (17-19). Table I summarizes the key peaks found in the N 1s and Fe $2p_{2/3}$ spectra obtained in a previous work (21). Both the N 1s and Fe $2p_{2/3}$ spectra are nearly identical suggesting that the active sites of the catalyst remains unchanged when acid leached and re-pyrolyzed. The majority of the surface nitrogen is shown to exist as pyridinic nitrogen (398.08 eV) and graphitic nitrogen (400.88 eV)(22-25) while the surface iron is shown to mainly exist in an ionic state (Fe(II) (708.13 eV) and Fe(III) (710.64 eV)) (23,24).

TABLE I. N 1s and Fe $2p_{2/3}$ XPS peaks for both catalysts.

Sample	N 1s [eV]	Fe $2p_{2/3}$ [eV]
FePAN4-900	398.12	708.13
	399.49	710.64
	400.89	713.73
	402.58	
FePAN4-900-AH	398.12	708.03
	399.49	710.50
	400.89	713.29
	402.58	

BET analysis

As discussed in previous sections, the electrochemical characterization and XPS spectra of the catalysts suggest that the acid leaching and re-pyrolysis of the catalyst results largely in a physical change of the microstructure of the catalyst, leaving the structure of the active site intact. To confirm this, the BET nitrogen adsorption/desorption isotherms of the FePAN4-900 and FePAN4-900-AH catalysts were

obtained and analyzed. The isotherms of the two catalysts can be seen in figure 4 while table II summarizes the BET surface area, average pore size, and micropore volume measurements obtained from the isotherms.

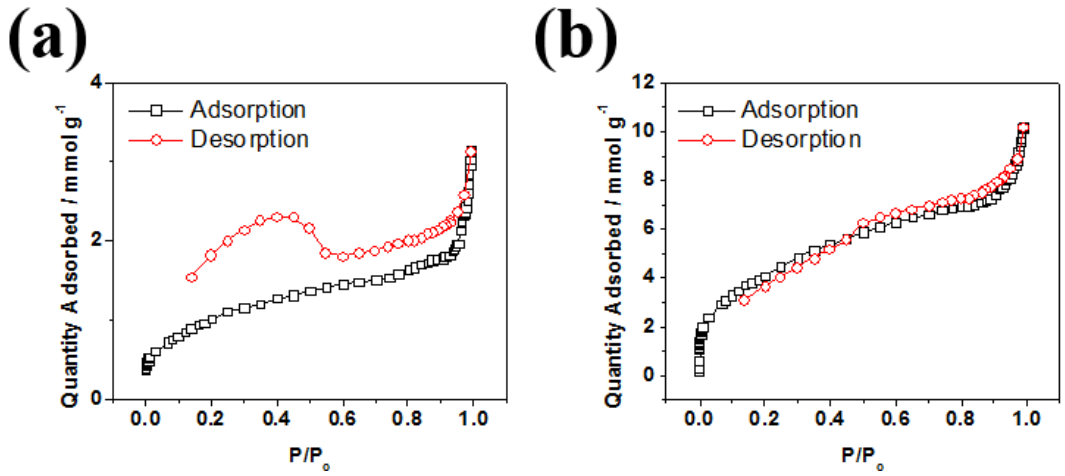

Figure 4. BET nitrogen adsorption/desorption isotherms of (a) FePAN4-900 and (b) FePAN4-900-AH catalysts.

TABLE II. BET surface area, pore size, and micropore volume analysis.

Sample	BET Surface Area [m^2/g]	Average Pore Size [nm]	Micropore volume [cm^3/g]
FePAN4-900	82.44	4.30	0.019
FePAN4-900-AH	339.11	6.57	0.069

Analysis of the isotherms shows a significant increase in BET surface area after acid leaching and re-pyrolysis of the FePAN4-900 catalyst. Additionally, a slight increase in the average pore size of the catalysts can be observed in the FePAN4-900-AH catalyst. Taken together, the increase in both the BET surface area and the average pore size suggests that the FePAN4-900-AH catalyst exhibits a more porous structure over the FePAN4-900 catalyst. This increase in porosity in the structure of the catalyst can allow for higher exposure of the micropores of the catalyst to reactants and is observed as an increase in the micropore volume in the FePAN4-900-AH catalyst. Based on previous published results, there is evidence that suggests that the active site of the catalyst may exist within the micropores of the carbon structure (17,19). In that case, the increase in micropore volume is synonymous with an increase in the exposure of ORR active sites. This increase in a higher effective ORR active site density accounts for the improvement in ORR catalytic activity seen in the FePAN4-900-AH catalyst.

Conclusion

A new type of nanofibrous non-precious pyrolyzed ORR catalysts for the PEMFC is presented and evaluated in the present work. The nanofibrous morphology of the catalysts was obtained by electrospinning a solution of iron acetate and polyacrylonitrile. After stabilization in air and high temperature pyrolysis, ORR active carbon nanofibers

were produced. Significant improvement in the ORR activity of the carbon nanofibrous catalysts was obtained after acid leaching and re-pyrolysis of the catalysts. The increase in ORR activity is thought to be due to a modification of the microstructure of the carbon nanofibers. The acid leached and re-pyrolyzed catalyst exhibits higher BET surface area and larger micropore volume, which suggests that the treatment results in higher porosity and thus increased exposure of micropores where the ORR active sites are located. The durability of the catalyst in the harsh acidic media is an additional concern and will be investigated in a future work. Additionally, the effects of the acid treatment on the durability of the catalysts could provide additional insight and will be pursued.

Acknowledgments

This work was financially supported by the Natural Sciences and Engineering Research Council of Canada (NSERC), the University of Waterloo and the Waterloo Institute for Nanotechnology.

References

1. V. Mehta and J. S. Cooper, *J. Power Sources,* **114**, 1 (2003).
2. J. Herranz, F. d. r. Jaouen, M. Lefeì€vre, U. I. Kramm, E. Proietti, J.-P. Dodelet, P. Bogdanoff, S. Fiechter, I. Abs-Wurmbach, P. Bertrand, T. M. Arruda and S. Mukerjee, *J. Phys. Chem. C,* **115**, 32 (2011).
3. C. W. B. Bezerra, L. Zhang, K. C. Lee, H. S. Liu, A. L. B. Marques, E. P. Marques, H. J. Wang and J. J. Zhang, *Electrochim. Acta,* **53**, 15 (2008).
4. Z. Chen, D. Higgins, A. Yu, L. Zhang and J. Zhang, *Energy Environ. Sci.,* **4**, 9 (2011).
5. G. Wu, K. L. More, C. M. Johnston and P. Zelenay, *Science,* **332**, 6028 (2011)
6. R. Jasinski, *Nature,* **201**, 492 (1964).
7. W. M. Li, A. P. Yu, D. C. Higgins, B. G. Llanos and Z. W. Chen, *J. Am. Chem. Soc.,* **132**, 48 (2010).
8. K. Wiesener, *Electrochim. Acta,* **31**, 8 (1986).
9. A. Fuhrmann, K. Wiesener, I. Iliev, S. Gamburzev and A. Kaisheva, *J. Power Sources,* **6**, 1 (1981).
10. A. L. Bouwkamp-Wijnoltz, W. Visscher and J. A. R. van Veen, *Electrochim. Acta,* **43**, 21-22 (1998).
11. G. Faubert, R. Cote, D. Guay, J. P. Dodelet, G. Denes and P. Bertrand, *Electrochim. Acta,* **43**, 3-4 (1998).
12. G. Faubert, G. Lalande, R. Cote, D. Guay, J. P. Dodelet, L. T. Weng, P. Bertrand and G. Denes, *Electrochim. Acta,* **41**, 10 (1996).
13. G. Lalande, R. Cote, G. Tamizhmani, D. Guay, J. P. Dodelet, L. Dignardbailey, L. T. Weng and P. Bertrand, *Electrochim. Acta,* **40**, 16 (1995).
14. G. Lalande, G. Tamizhmani, R. Cote, L. Dignardbailey, M. L. Trudeau, R. Schulz, D. Guay and J. P. Dodelet, *J. Electrochem. Soc.,* **142**, 4 (1995).
15. S. Gupta, D. Tryk, I. Bae, W. Aldred and E. Yeager, *J. Appl. Electrochem.,* **19**, 1 (1989).
16. X. Li, B. N. Popov, T. Kawahara and H. Yanagi, *J. Power Sources,* **196**, 4 (2011).
17. M. Lefevre, E. Proietti, F. Jaouen and J. P. Dodelet, *Science,* **324**, 5923 (2009).

18. J. Herranz, F. Jaouen and J.-P. Dodelet, *ECS Trans.,* **25**, 1 (2009).
19. F. Jaouen, M. Lefevre, J. P. Dodelet and M. Cai, *J. Phys. Chem. B,* **110**, 11 (2006).
20. G. Lalande, R. Cote, D. Guay, J. P. Dodelet, L. T. Weng and P. Bertrand, *Electrochim. Acta,* **42**, 9 (1997).
21. J. Wu, H. W. Park, A. Yu, D. Higgins and Z. Chen, *J. Phys. Chem. C,* **116**, 17 (2012).
22. P. H. Matter, L. Zhang and U. S. Ozkan, *J. Catal.,* **239**, 1 (2006).
23. C. W. B. Bezerra, L. Zhang, K. C. Lee, H. S. Liu, J. L. Zhang, Z. Shi, A. L. B. Marques, E. P. Marques, S. H. Wu and J. J. Zhang, *Electrochim. Acta,* **53**, 26 (2008)
24. R. L. Arechederra, K. Artyushkova, P. Atanassov and S. D. Minteer, *ACS Appl. Mater. Interfaces,* **2**, 11 (2010).
25. F. Jaouen, J. Herranz, M. Lefeì€vre, J.-P. Dodelet, U. I. Kramm, I. Herrmann, P. Bogdanoff, J. Maruyama, T. Nagaoka, A. Garsuch, J. R. Dahn, T. Olson, S. Pylypenko, P. Atanassov and E. A. Ustinov, *ACS Appl. Mater. Interfaces,* **1**, 8 (2009).